CHEMISTRY OF MATERIALS

pubs.acs.org/cm

Article

Elucidating the Impact of *Cis*–*Trans* Organic Structure Directing Agent Isomer Ratios on the Aluminum Distribution Within SSZ-39

Charles E. Umhey, Jiawei Guo, Zheng Cui, Daniel F. Shantz, Ambarish Kulkarni, and Jean-Sabin McEwen*

Cite This: *Chem. Mater.* 2024, 36, 11852–11862

Read Online

ACCESS | Metrics & More | Article Recommendations | Supporting Information

ABSTRACT: Despite their widespread use, the mechanisms governing the synthesis of zeolite catalysts are still poorly understood. A notable example of this problem is the uncertainty surrounding the influence of synthesis conditions on the placement of Al atoms in the zeolite framework, which determines the active sites available for catalytic species. In this work, the role of the *cis* to *trans* isomer ratio of the OSDA *N*,*N*-dimethyl-3-5-dimethylpiperidinium on the energetics of 26 distinct Al pair distributions in SSZ-39 is examined both in the presence and absence of Na using density functional theory calculations. The initial orientation of the OSDA was found to have a significant impact on the final energies present, necessitating the screening of a large number of initial orientations with force field calculations and single point DFT calculations. Ground state energies were found to vary significantly with the ratio of *cis* to *trans* OSDAs with a Boltzmann distribution revealing the most likely Al pair distributions shift from sharing the same 8 membered rings to sharing the same double 6-membered rings to having no shared subunits as one increases the amount of *cis* OSDA present within the framework. The presence of Na was found to favor Al pair distributions where both Als occupied the same 6-membered ring. When an implicit solvent model was used to evaluate ground state energies the ideal Na sites shifted from 6-membered rings to empty SSZ-39 cages while OSDA positions and orientations remained largely the same. To provide insight on how kinetic factors may influence Al distributions, formation energies we calculated for connected double 6-membered rings. These formation energies revealed a preference for Al pairs to occupy the same 4-membered ring, which indicates kinetic and thermodynamic control may lead to different Al distributions in SSZ-39.

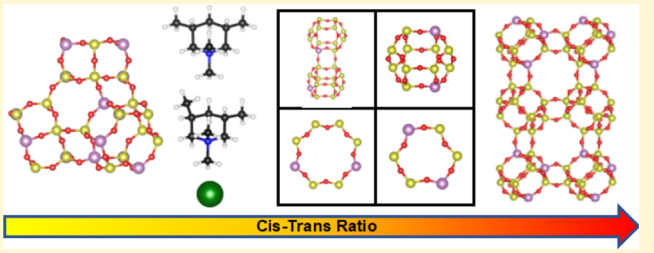

1. INTRODUCTION

Zeolites are microporous aluminosilicate materials with widespread uses in petroleum refining,[1] ion exchange processes,[2] and NO_x removal.[3] Replacing a Si species in a zeolite framework with an Al atom creates a charge deficit which enables the placement of a positively charged catalytically active species such as copper. The exact location of these Al atoms in zeolite frameworks can have a significant impact on the catalytic activity of the zeolite.[4] Al atoms in zeolite frameworks can be located quite close to each other in pairs separated by only one or two silicon atoms. These pairs have been shown to increase NH_3 catalytic activity toward the selective catalytic reduction of NO_x gases in copper exchanged zeolites by promoting the redox cycle of Cu ions.[5] One particularly promising zeolite for NO_x reduction is SSZ-39 which has shown exceptional hydrothermal stability and high activity toward the selective catalytic reduction of NO_x gases.[6] These properties position SSZ-39 as a potential next generation catalyst for SCR.

Unfortunately, despite the importance of Al pairs for zeolite catalysts the mechanisms governing Al distributions in zeolites are still poorly understood. Recent work by the Shantz group has suggested organic structure directing agents may play a key role in Al distribution in zeolites. During the synthesis of zeolites, organic structure directing agents are commonly used to select for certain zeolite frameworks and Al distributions.[7] The Shantz group has found that altering the ratio of the *cis* to *trans* isomer of the OSDA *N*,*N*-dimethyl-3-5-dimethylpiperidinium (depicted in Figure 2) can alter both the catalytic activity and the copper uptake of Cu-SSZ-39,[8] during the interconversion of faujasite (FAU) to SSZ-39. The Shantz group also found the *trans* isomer increases the synthesis speed and increases the Si/Al content of SSZ-39.[9] Other publications have reported similar results indicating the *trans* isomer has been observed to both result in faster crystallization and be preferentially uptaken over *cis* isomers.[10] These results suggest the interconversion of FAU to SSZ-39 can be a model system

Received: August 2, 2024
Revised: November 14, 2024
Accepted: November 15, 2024
Published: December 6, 2024

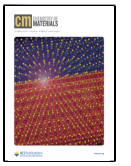

to study the influence of interactions between the OSDA and the zeolite and how it affects the catalytic properties through the preferential placements of Al within the zeolite framework.

We investigate this phenomenon of OSDA isomer ratio influencing the Al distribution by comparing the energetics of Al pairs when charge compensated by different combinations of *cis* and *trans* OSDA isomers in the presence and absence of sodium, using density functional theory calculations. Prior work has shown differences in the DFT calculated binding energy between zeolite frameworks and OSDAs can be used to make predictions about Al distributions matching experimental results.[11] Other works by Schneider and coworkers on SSZ-13 also looked at the influence of the OSDA *N,N,N*-trimethyl-1-adamantyl ammonium on the Al distribution by using *ab initio* molecular dynamics, classical force field calculations and classical molecular dynamics simulations[12] concluding that electrostatic interactions between OSDA charge centers and Al play a significant role in determining the energetics of zeolite−OSDA systems. In other work the Schneider group showed that the coadsorption of Na cations with OSDA molecules altered the Al distributions in SSZ-13 by making Al pairs in 6-membered rings more favorable.[13]

SSZ-39 has 4 subunits capable of housing Al pairs, 4-membered rings (4MR), 6-membered rings (6MR), double 6-membered rings (D6MR), and 8-membered rings (8MR) (see Figure 1). 4MR, 6MR and D6MR subunits are also found in

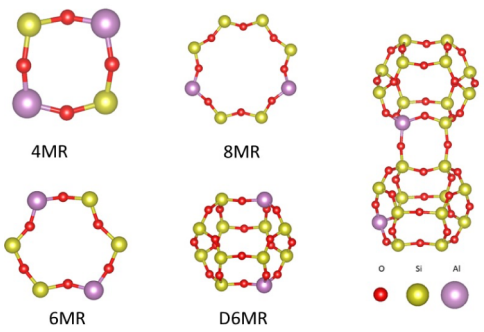

Figure 1. SSZ-39 subunits capable of housing Al pairs and an Al pair occupying no shared units.

FAU and whether these subunits are preserved or dissolved during synthesis is still the subject of debate.[14−16] The distribution of Al pairs and the subunit housing an Al pair can have a significant influence of the catalytic activity of the active site.[17−19] In this work, we use a local minimum screening method with both classical force fields and DFT-based calculations to determine how the OSDA isomer ratio and the coadsorption of Na influences Al pair distributions in SSZ-39 Figure 2. By evaluating what OSDA isomers favor certain Al distributions we can offer a potential explanation for why

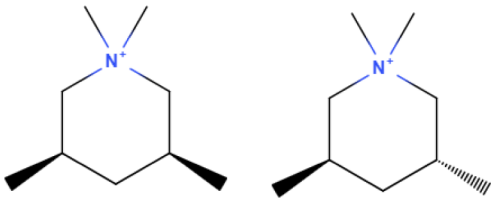

Figure 2. *Cis* (left) and *Ttrans* (right) isomers of *N,N*-dimethyl-3-5-dimethylpiperdinum.

altering the OSDA isomer alters catalytic properties and offer a way to tailor zeolites for specific reactions.

2. METHODS

2.1. Force Field Calculation Details. All force field calculations were performed using the Large-scale Atomic/Molecular Massively Parallel Simulator (LAMMPS) software package.[20] The Dreiding[21] force field was used to model atoms permanently bonded together which has been shown to be effective at modeling zeolite-OSDA systems. To model interactions between unbonded atoms we used Lennard-Jones parameters that had been optimized for interactions between CHA frameworks and *N,N,N*-trimethyl-1-adamantyl ammonium, as well as sodium and FAU frameworks.[22,23] In our models the atoms in the zeolite framework were fixed in place and the OSDA molecules were rigid. In order to examine the effectiveness of our force field models in accurately calculating the energetics of zeolite OSDA pairings we randomly selected a zeolite OSDA pair and used VASP to calculate the energy of the optimized configurations for each of the 1000 configurations screened by LAMMPS and compared the relative energies (Figure S2). The results indicated a strong correlation between energies calculated by LAMMPS and energies calculated by VASP, giving us confidence LAMMPS could be used to identify promising initial configurations.

2.2. DFT Calculation Details. All density functional theory calculations were performed using the Vienna *Ab initio* Simulation Package (VASP) version 6.[24−27] The interactions between valence and core electrons were modeled using the projector augmented wave method,[28] using PAW potentials released by VASP developers in 2017. The optB86b-vdW exchange correlation functional was used for all VASP calculations.[29] Initially a 1 × 1 × 1 KPOINT mesh was used to sample the Brillouin zone with Gaussian smearing with a width of 0.2 eV. After geometries were converged with a 1 × 1 × 1 mesh the structures were then reoptimized with a 2 × 2 × 1 KPOINT mesh. Self-consistent field cycles were considered converged once the total energy difference between steps was less than 1×10^{-5} eV. Geometries were considered converged when the norms of all forces were smaller than 0.02 eV/Å. Since spin polarized calculations converged to negligible magnetic moments, we preformed all calculations without spin polarization. The lattice parameters for our unit cell were identified by optimizing atomic coordinates while also allowing the cell shape to relax with a variety of different scaling factors and selecting the lattice parameters that minimized the final energy. These calculations identified an optimal cell volume of 1592.76 Å^3 (a = 9.23 Å, b = 9.43 Å, c = 18.36 Å, α = 90.14, β = 89.64, g = 94.57) using the optB86b-vdW functional. A volume energy curve for our system can be seen in Figure S3. Entropy was calculated using the partition function as implemented by vaspkit.[30] To account for solvent effects an implicit model was implemented using VASPsol.[31−33] In this implicit solvation model relative permittivity for water was set to 78.4 to simulate the effects of an aqueous environment.

2.3. Al Distribution Generation. To generate SSZ-39 frameworks we acquired the SSZ-39 framework structure from the international zeolite association database of zeolite frameworks.[34] We then converted the atomic coordinates to the Niggli reduced cell using the Visualization for Electronic and Structural Analysis (VESTA) software. We then used the Multiscale Atomistic Zeolite Simulation Environment software package[35] to generate all unique Al pair distributions in our unit cell that obey Löwensteins rule.

2.4. Local Minima Screening. To minimize the impact of local minima we used three strategies to generate initial OSDA positions inside SSZ-39 ensuring each Al pair and charge compensating species had at least three initial positions and allowing us to evaluate the effectiveness of different strategies for calculating OSDA−zeolite interactions.

In the first method, we used chemical intuition to orient the OSDA molecules with their charge centers facing the Al atoms in the SSZ-39 framework while attempting to minimize the interactions between the OSDA and the rest of the framework. In the second method, we used

https://doi.org/10.1021/acs.chemmater.4c02175
Chem. Mater. 2024, 36, 11852−11862

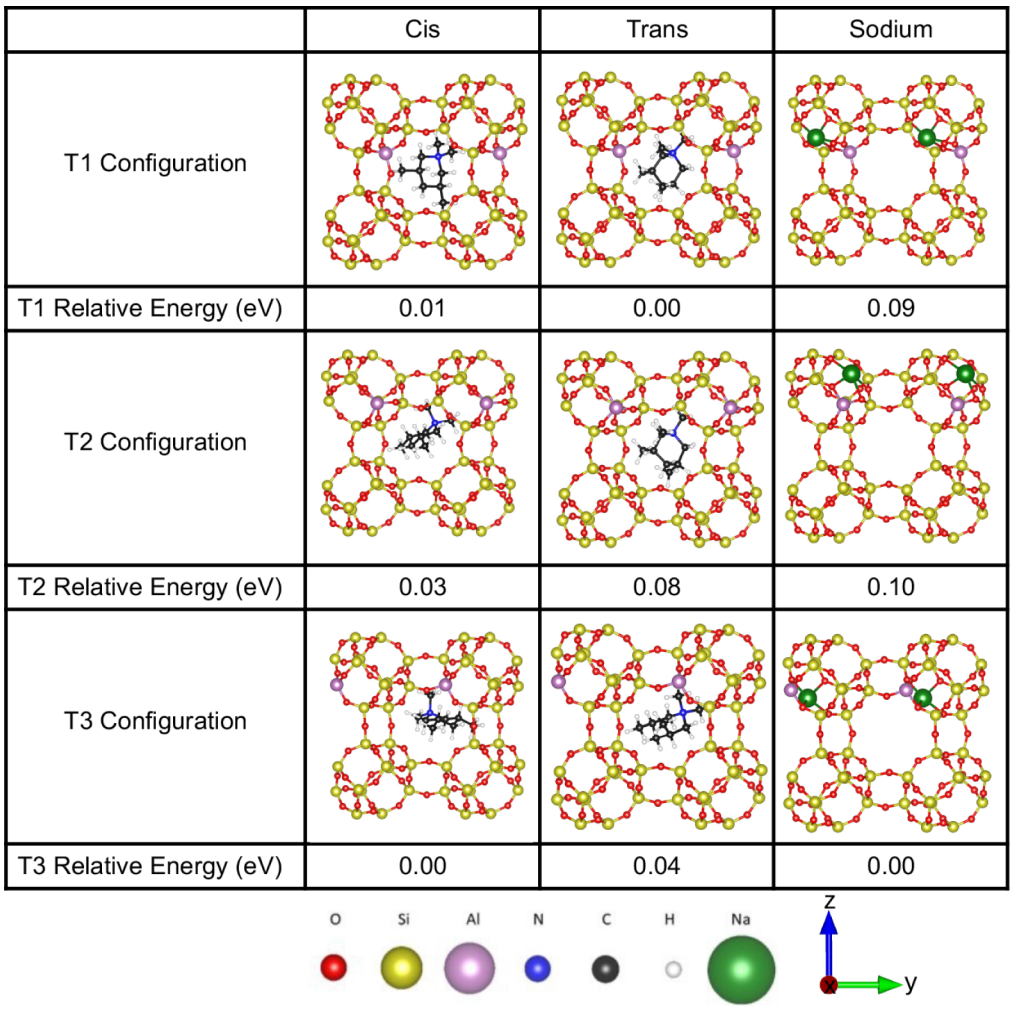

Figure 3. Most favorable positions for each charge compensating species in each T site in SSZ-39.

the LEGO[36−38] module of the Northwest Potential Energy Surface Search Engine (NWPEsSE)[36−38] to generate 100 random initial configurations for each system. These systems were then screened using single point calculations in VASP to identify the most promising initial configuration. The most energetically favorable configuration generated by LEGO for each system was then fully optimized in VASP. In our third method, we again used LEGO to generate initial configurations however in this method we screened the initial configurations by performing a geometry optimization with force field calculations using LAMMPS before selecting the most favorable initial configuration for a full geometry optimization with DFT-based calculations. Since force field calculations are inexpensive relative to DFT calculations, we were able to test 1000 initial configurations per system using this method.

2.5. Distortion Energy Calculation. To calculate the distortion energy, we first calculated the energies and configurations of each OSDA isomer in the gas phase using a pacifying background charge to account for the charge of the OSDA. We then took the converged structures with OSDA molecules in the SSZ-39 framework and deleted the zeolite framework leaving only the OSDA remaining. A single point calculation was then performed on the resulting structure with a pacifying background charge. The distortion energy was then calculated as the difference between the ideal gas phase configuration of the OSDA and the configuration the OSDA assumed in the SSZ-39 framework:

$$E_{\text{distortion}} = E_{\text{gas phase OSDA}} - E_{\text{OSDA in zeolite}} \quad (1)$$

2.6. Boltzmann Distribution Calculation. Once the energies had been calculated for each OSDA-zeolite pair a Boltzmann distribution was calculated for each Al pair at the synthesis temperature of 413 K using standard statistical mechanics techniques. The probability of a given state i, is given by

$$P_i = \frac{e^{-\frac{\epsilon_i}{k_B T}}}{\sum_{j=1}^{M} e^{-\frac{\epsilon_j}{k_B T}}} \quad (2)$$

where k_B is Boltzmann's constant, T is temperature, ϵ_i represents the energy of the system for conformation i and M is the number of conformations considered.

2.7. Formation Energy Calculations. To calculate the formation energy of connected D6MR subunits we first optimized isolated D6MR subunits in the gas phase. When Al was present Na was added as a charge compensating species to each 6MR containing Al. In cases where two Al atoms were present in the same 6MR the second Na was added to the other 6MR in the D6MR containing the 6MR with both Al atoms. Each D6MR subunit was capped with hydrogen atoms to ensure each T site had 4 bonds.

Formation energies are defined according to the equation below

$$E_f = E(\text{2D6MR}) - E(\text{D6MR}_A) - E(\text{D6MR}_B) - E(O_2) + 2E(H_2)$$

Where E(2D6MR), E(D6MR$_A$), E(D6MR$_B$), E(O_2), $2E$(H_2) are the energies of the 2D6MR structure, the first and second D6MR subunits isolated in the gas phase, and of oxygen and hydrogen which are added or released to enable the joining of both D6MRs, respectively.

https://doi.org/10.1021/acs.chemmater.4c02175
Chem. Mater. 2024, 36, 11852−11862

3. RESULTS

3.1. Preferred T Site for OSDA and Sodium Binding. When examining the relative energies of *cis* and *trans* OSDAs in SSZ-39 with 1 Al atom per unit cell, the *cis* OSDA appears to have no preference for the T site the Al atom occupies. Relative energies only vary by 0.03 eV when the Al atom is moved from the most favorable T3 site to the least favorable T2 site. In contrast *trans* OSDAs have a slightly higher range of relative energies with a 0.08 eV energy difference between the most favorable T1 site and the least favorable T2 site.

As can be seen from Figure 3, the most favorable orientation of the OSDA within the SSZ-39 cage depends on the T site occupied by the Al atom. As the T site containing Al changes from T1 to T3 the orientation of the OSDA shifts from having its ring aligned parallel to the *z* axis to having its ring aligned perpendicular to the *z* axis. For T1 sites both *cis* and *trans* OSDAs orient to be parallel to the *z* axis. With respect to T2 sites the ideal orientation depends on the isomer of the OSDA with *cis* OSDAs preferring a 45-degree angle with the *z* axis, and *trans* OSDAs preferring a parallel orientation to the *z* axis. With a T3 site, the *cis* OSDAs orient themselves to be perpendicular to the *z* axis while *trans* OSDAs prefer a 45-degree angle with respect to the *z* axis. For all T sites Na is found to bind most favorably in a 6-membered ring with the T3 site being the most favorable position for the Al atom by 0.092 and 0.099 eV compared to the T1 and T2 sites, respectively.

3.2. Local Minima and OSDA Orientation. Our initial results revealed small variations in the initial orientation of the OSDA molecules can have large impacts on final energies. By placing a single OSDA in SSZ-39 with one Al atom per unit cell we were able to obtain energy differences between the final optimized structures of up to 0.72 and 0.29 eV with *cis* and *trans* OSDAs, respectively. Interestingly, the configurations with *cis* OSDAs had a significantly higher standard deviation than configurations with *trans* OSDAs (~0.3 eV vs ~0.05 eV) suggesting the placement of the *cis* OSDAs had a large impact on stability. The presence of these local minima necessitates the sampling of multiple initial orientations for each configuration. When testing configurations with only one OSDA and one Al atom present the number of possible orientations is small enough to sample all possible orientations without excessive computational costs. However, when multiple OSDAs are present a huge number of permutations of each OSDA orientation becomes available to the system making sampling each possible configuration with DFT calculations unfeasible. To resolve this issue, we developed three methods of determining OSDA orientation in SSZ-39 that minimize computational expense while still exploring a large configurational space. Each method is discussed in detail in Section 2.4. The force field screening method proved the most effective at identifying minimum energy configurations with 51% of all minimum energy configurations being identified by force field screening while single point screening and chemical intuition performed equivalently to each other identifying 26% and 23% of all minimum energy configurations respectively (see Figure 4).

A fourth method was considered where we took the most favorable orientations for each OSDA when charge compensating an isolated Al atom and using those orientations for pairs of OSDA molecules when charge compensating an Al pair. To determine if this approach was worth testing we used it on the most favorable Al distribution for each charge compensating species. For configurations with two OSDA molecules the resulting configurations had higher energies than the previous minima, which had orientations counter to what we would expect based on the orientations for the one Al per unit cell systems, as illustrated in Figure 5. Additionally, when examining the final orientations of OSDAs for each Al distribution studied, a wide range of orientations can be found for each charge compensating species suggesting the ideal orientation is influenced by interactions between OSDA molecules as well as framework−OSDA interactions. Despite the failure of this method with multiple OSDA molecules, in systems with Na and OSDA molecules present placing Na cations in their preferred 6MR positions and reorienting the OSDA molecules to their ideal orientation for an isolated Al site was incredibly successful at finding new minima. This strategy identified lower energy configurations than all other methods of initial point generation 87% of the time.

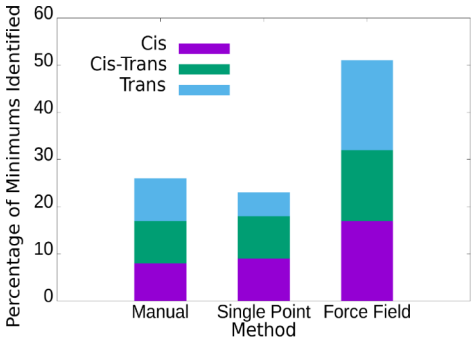

Figure 4. Percentage of local minima identified by each method for configurations with two OSDAs per unit cell.

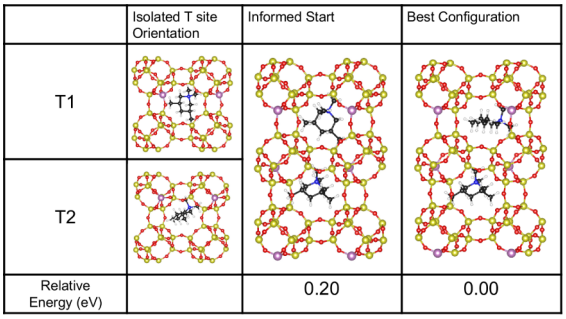

Figure 5. Ideal configurations for *cis* OSDAs with isolated Al sites and optimized configurations with OSDAs initial positions matching ideal orientations (method 4 described in the text) or the best configurations identified by our other screening methods. The sphere legend is the same as Figure 3.

3.3. OSDA Distortion. Our results show configurations containing 2 OSDAs in the same cage are dramatically less favorable (4.5 eV on average) than configurations where only one OSDA occupies each cage. Experimentally Si:Al ratios for SSZ-39 made with *N*,*N*-dimethyl-3-5-dimethylpiperidinium range from 9.7:1 to 10.0:1[8] which is slightly lower than the Si:Al ratio of 11:1 used in our calculations. This slightly lower ratio means some SSZ-39 cages will have two Al atoms. The extreme unfavorability associated with having two OSDAs occupy the same cage leads us to conclude in order to achieve the slightly higher Al content observed experimentally, the additional Al must be charge compensated by Na, since Si:Al

https://doi.org/10.1021/acs.chemmater.4c02175
Chem. Mater. 2024, 36, 11852−11862

ratios below what we model require more than one charge compensating species per cage. This conclusion is reinforced by prior work from Dusselier and coworkers which has shown via TGA analysis that as-made SSZ-39 contains at most one OSDA per cage.[10] One likely cause of this phenomenon is the need for OSDA molecules to deviate from their ideal gas phase geometries to accommodate the other OSDA (Figure 6). To

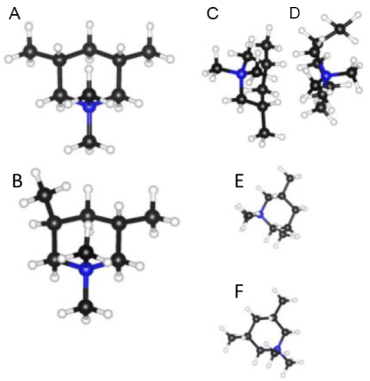

Figure 6. Gas phase *cis* (A) and *trans* (B) OSDA configurations compared to *cis* (C) and *trans* (D) OSDAs forced to occupy the same cage and *cis* (E) and *trans* (F) OSDAs allowed to occupy separate cages.

test this hypothesis, we calculated the distortion energy of each system tested and compared the distortion energies of configurations with multiple OSDAs occupying the same cage to the distortion energy of configurations with each OSDA occupying separate cages. Our results found an average difference in distortion energy of 2.57 eV between OSDA pairs in the same cage vs OSDA pairs in separate cages. This energy difference accounts for 57% of the difference between same and separate cage configurations. The remaining discrepancy is likely due the OSDAs being located closer to the zeolite framework due to the limited space inside each cage. While the distortion energy can explain why same cage configurations are less favorable than separate cage configurations, there is no correlation between the distortion energy and the energy differences between configurations where both configurations have OSDAs in separate SSZ-39 cages indicating the differences are due to other factors such as interactions between the framework and the OSDA.

3.4. Effect of Charge Compensating Species on Ground State Energies of SSZ-39 with Different Al Pair Distributions. In order to test the effect of charge compensating species on the ground state energies of different Al distributions in SSZ-39, we calculated the ground state energy of each Al pair distribution when charge compensated by two *cis* OSDAs, one *cis* OSDA and one *trans* OSDA, two *trans* OSDAs, one Na cation and a *cis* OSDA, and one Na cation and one *trans* OSDA. As seen from Figure 7, when two Al atoms are present, varying the Al pair distribution or the charge compensating species can lead to significant changes in ground state energies. Additionally, when a Boltzmann distribution was calculated at the synthesis temperature of 413 K it can be seen that the charge compensating species has a significant impact on the most likely Al distributions (see Figure 8).

As can be seen from Figure 9, the preferred Al pair distribution shifts from occupying no shared subunits, to occupying the same D6MR, to occupying the same 8MR as the

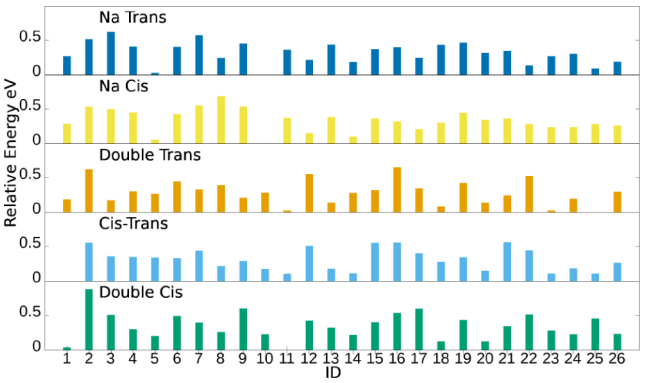

Figure 7. Relative energies for each Al distribution with each charge compensating species. Energies are relative to the minimum energy which has been set to zero.

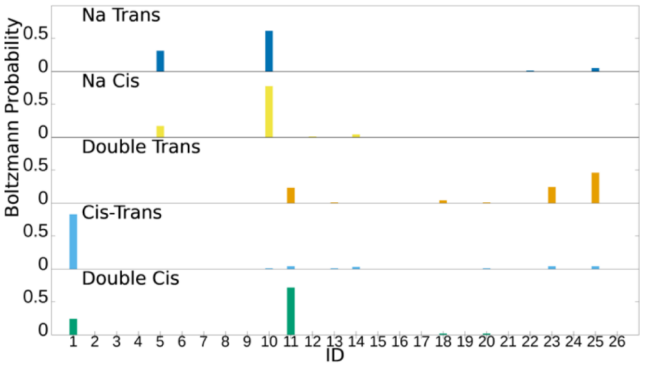

Figure 8. Boltzmann probabilities for Al distributions with each charge compensating species at 413 K.

System	Cis	Cis-Trans	Trans	Cis-Na	Trans-Na
Geometry	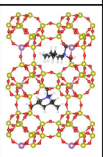	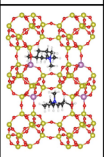	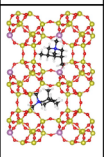	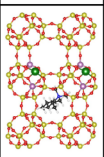	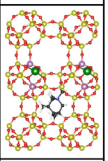
Al Distribution	Separate	D6MR	8MR	6MR	6MR
Probability	0.71	0.82	0.46	0.77	0.61

Figure 9. Most probable Al distributions for each charge compensating species and the probability of observing each Al distribution with the given charge compensating species based on a Boltzmann distribution at 413 K. The sphere legend is as in Figure 3.

charge compensating species changes from exclusively *cis* OSDAs, to a 50:50 mixture, to exclusively *trans* OSDAs. When Na is coadsorbed with either *cis* or *trans* OSDA the same 6MR distribution is found to be most favorable. Interestingly, work by the Schneider group investigating the coadoption of the OSDA *N,N,N*-trimethyl-1-adamantylammonium and Na cations in the CHA framework found similar results with the coadsorption of OSDA molecules and Na cations leading to the formation of Al pairs in 6MR subunits.[13]

These findings indicate that altering the *cis* to *trans* ratio as well as the Na content of the synthesis mixture can be used to influence the most thermodynamically favorable Al distribution of SSZ-39. The favorability of different Al distributions when charge compensated by a background charge does not have any correlation with the favorability of the same Al distributions when charge compensated by any of the charge

https://doi.org/10.1021/acs.chemmater.4c02175
Chem. Mater. 2024, 36, 11852−11862

compensating species investigated (Figure S5). This suggests the differences in favorability observed among different Al pair distributions are due to the interactions between the charge compensating species and the framework rather than certain Al distributions being inherently more stable. Calculated changes in entropy were slightly negative and minimal with a slight decrease of around ∼−0.004 eV/K for all conformation that were considered.

3.5. Relationship between N−Al Distance and OSDA Binding Energy. Prior work with zeolites has shown a strong correlation between the distance of the charge center of the OSDA and the nearest Al atom and the ground state energy of the zeolite.[12] Interestingly we do not observe this relationship when examining our data (see Figure 10). One possible

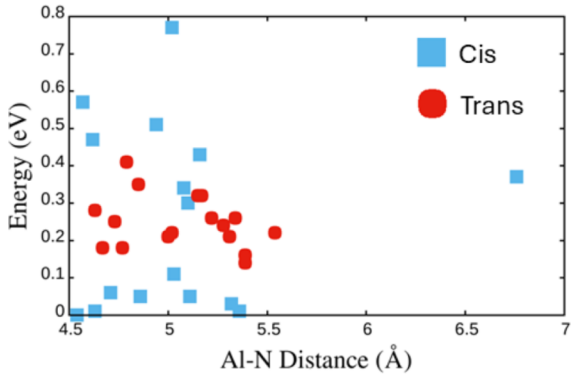

Figure 10. Ground state energy as a function of Al−N distance for systems with a single OSDA and Al atom per cage when all atoms in the OSDA are relaxed. Energies are relative to the minimum energy which has been set to zero.

explanation for this is that our OSDA is smaller than the OSDA cage and can reorient itself so the ideal N−Al distance is always maintained which is not possible with other OSDA-zeolite systems where the OSDA is much larger than the zeolite cage, such as *N,N,N*-trimethyl-1-adamantyl ammonium in chabazite. To test this hypothesis, we created a chargeless OSDA by replacing the nitrogen in the molecule with carbon. We then optimized the chargeless OSDA in SSZ-39 with no aluminum (see Figure S6). This enabled us to determine the ideal orientation for the *cis* and *trans* OSDA before Al−N interactions are accounted for. We then added the nitrogen back to the OSDA and froze the molecule in the ideal position and calculated the ground state energies for several different Al locations. When the OSDA is not allowed to rotate we see a clear relationship between OSDA−N distance and ground state energy. This relationship becomes even stronger when we look at individual T sites (see Figure 11). This preference for minimizing the Al−N distance is likely why our systems have an Al−N distance between 4.5 and 5.5 Å. At this distance we observe favorable Al−N interactions, and the ground state energy is influenced by other factors such as OSDA−framework interactions.

3.6. Effect of Solvation on OSDA Binding. In experimental conditions the synthesis of SSZ-39 takes place in an aqueous medium. To account for this, we reoptimized each zeolite-OSDA system using an implicit solvation model to account for water present during synthesis. This implicit solvation model had little impact on the results for systems with exclusively OSDAs as charge compensating species. These systems averaged a change in relative energy of only 0.045 eV

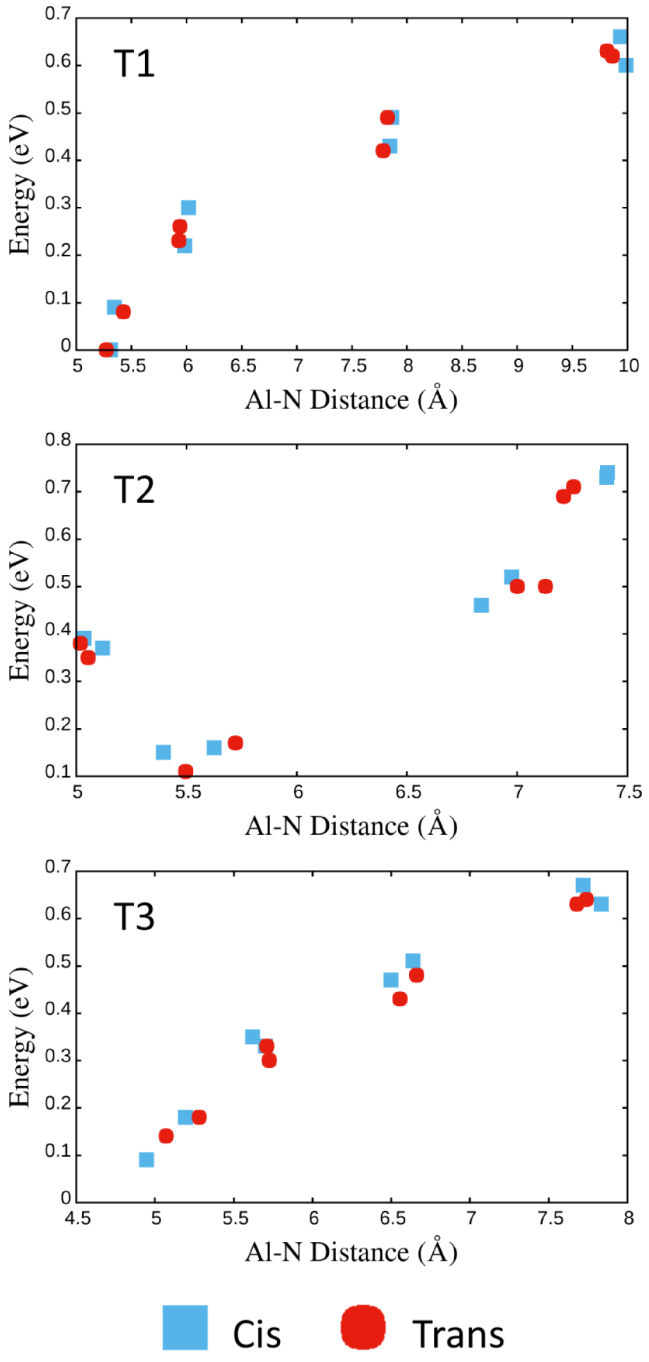

Figure 11. Ground state energy as a function of Al−N distance for systems with a single OSDA and Al atom per cage when the OSDA is frozen in its ideal orientation for a chargeless system. Energies are relative to the minimum energy which has been set to zero.

with no significant change in the final positions or orientations for the OSDAs. No change was observed in which aluminum distribution was most favorable for the exclusively *cis* exclusively *trans*, or 50:50 *cis*:*trans* systems. Relative energies for solvated systems were found to correlate strongly with relative energies for unsolvated systems (Figure 12).

When examining systems with Na present the implicit solvation model has a significant impact on our results. When sodium is present in solvated systems a shift in the position of Na atoms inside SSZ-39 is observed. In systems without implicit solvation models Na atoms are most favorable in

https://doi.org/10.1021/acs.chemmater.4c02175
Chem. Mater. 2024, 36, 11852−11862

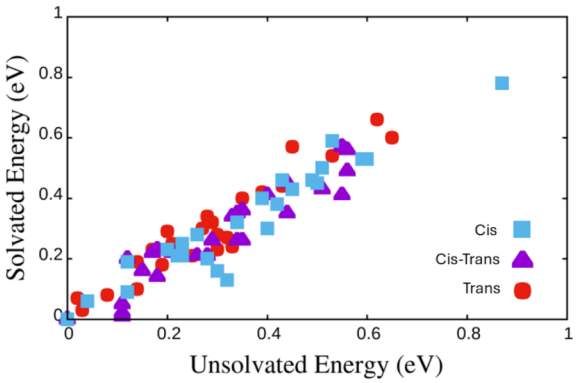

Figure 12. Energy of systems containing exclusively OSDAs with and without an implicit solvation model. Energies are relative to the minimum energy which has been set to zero.

6MRs and D6MRs containing Al atoms. When an implicit solvation model is added to the system Na atoms become mobilized leaving the 6MRs and instead occupying the cages within SSZ-39 (Figure 13). Exceptions to this trend can be

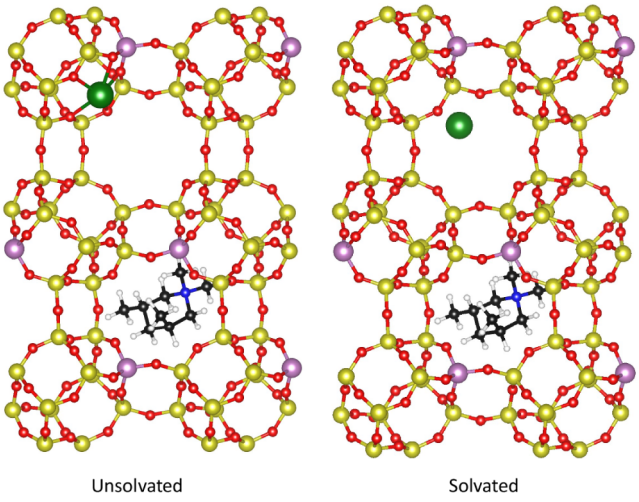

Figure 13. Optimized configurations for a *trans*-Na system with (right) and without (left) implicit solvation.

seen when OSDAs already occupy the cage that is adjacent to the 6MR which contains Na in the unsolvated model. In these systems, the sodium remains in the 6MR. This finding is in line with previous studies in the literature where it has been found that the mobility of Na species can be enhanced in the presence of water.[39,40] Na placed within a D6MR is unable to migrate into SSZ-39 cages regardless of whether or not an implicit solvation model is used. These shifts in Na position are accompanied by significant changes in energy with average relative energies changing by 1.6 eV for systems with sodium and *cis* OSDAs and 0.38 eV for systems with *trans* OSDAs and sodium atoms. Unlike systems with exclusively OSDA, relative energies of solvated systems do not strongly correlate with the relative energies of unsolvated systems (Figure 14). This lack of correlation between solvated and unsolvated relative energy is likely due to the shift in sodium atom positions which change the chemical environment of Na. When care is taken to group systems based on the location of the sodium atom so unsolvated and solvated energies are compared between systems where sodium has the same position a weak

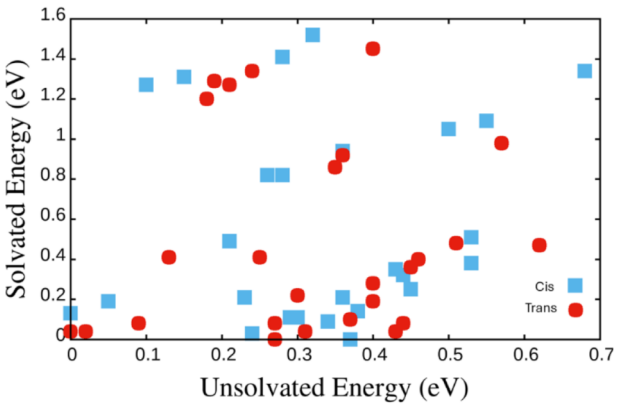

Figure 14. Energy of systems containing an OSDA and a sodium atom with and without an implicit solvation model. Energies are relative to the minimum energy which has been set to zero.

correlation can be observed between solvated and unsolvated energy among systems where the Na atom is located in 6MRs and D6MRs (Figure 15). The most favorable Al distributions in the presence of Na are altered by the implicit solvation model as compared those where there is no implicit solvation (as shown in Figure 9). In the *cis*-Na system, the most favorable Al distribution changes to a configuration where the Al atoms do not share a subunit, while in the *trans*-Na system the most favorable Al distribution changes to a configuration where the Al pair occupies an 8MR (see Figure 16).

3.7. Effect of Al Distribution on the Energetics of D6MR Connection. So far, this work has primarily evaluated how thermodynamic factors influence Al distributions in SSZ-39. While such thermodynamic approaches have had some success at predicting Al distributions in the literature[11] kinetic factors likely also influence the Al siting inside SSZ-39. While a complete kinetic analysis is beyond the scope of this paper, we can offer some insight into the kinetics of SSZ-39 nucleation by evaluating how different Al distributions influence the formation energy of possible intermediate species in the nucleation of SSZ-39. SSZ-39 is entirely constructed of connected double 6-membered rings that can be connected along the *Z* axis or the *XY* plane with slightly different geometries for each case. It has been argued in the literature that during the interconversion of FAU to other zeolite frameworks the D6MR subunits present in FAU remain intact.[15] This suggests the connection of two D6MR subunits may be a kinetically relevant step for the nucleation of SSZ-39.

We calculated the formation energy associated with connecting two D6MR subunits. Our results indicate the most favorable locations for Al when connecting D6MR subunits is within the 4-membered ring linking both D6MRs. Moving the Al atom to a position that is not part of the 4-membered ring linking both D6MRs increases the formation energy by ~0.44 eV indicating a clear preference for the Al to occupy the 4 membered ring joining double 6-membered rings (see Figure 17). This preference exists whether the rings are linked along the *Z* axis or along the *XY* plane. When a second Al atom is added the most favorable distribution has both Al atoms in the 4MR linking the D6MRs for both the *Z* axis link and the *XY* plane link, however moving one of the Al atoms to a site that is not part of the 4MR results in a significantly smaller change in energy of about 0.02 eV for the next most favorable position (see Figure 18) as compared to the 0.44 eV change in energy when only a single Al is present. When

https://doi.org/10.1021/acs.chemmater.4c02175
Chem. Mater. 2024, 36, 11852−11862

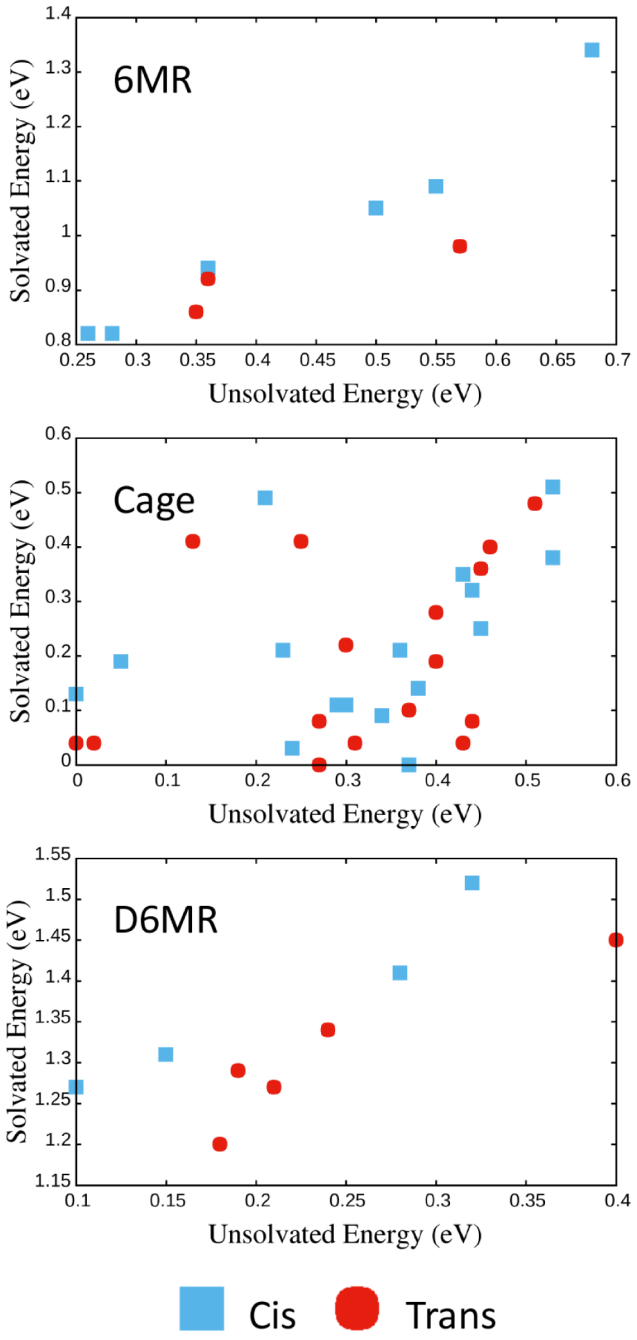

Figure 15. Energy of systems containing an OSDA and a Na cation with and without an implicit solvation model with systems grouped by the environment of Na in the optimized system with implicit solvation. Energies are relative to the minimum energy which has been set to zero.

comparing formation energies rather than total energies for 2Al systems a significant preference (~0.3 eV) is found for 2D6MR systems when both Al atoms occupy the 4MR linking both D6MR subunits. This can be attributed to systems with a pure silica D6MR in the gas phase and a 2AlD6MR in the gas phase being more stable than systems with two 1AlD6MRs in the gas phase which raises the formation energy. When examining the distribution of formation energies (see Figures S7 and S8) a gap can be seen where no structures exist with formation energies between −9.73 eV and −9.30 eV for systems with one Al and no structures exist with formation energies between

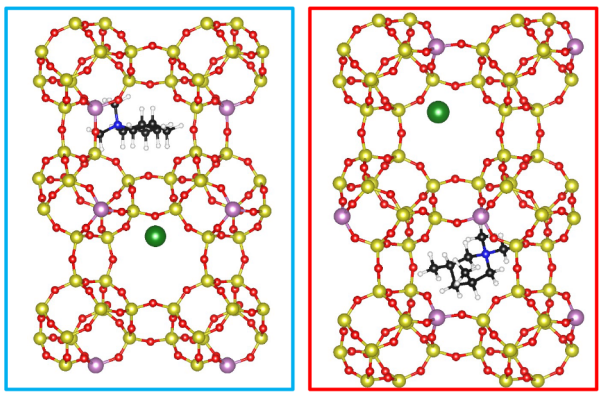

Figure 16. Most favorable Al distributions for *cis*-Na (left) and *trans*-Na (right) systems when an implicit solvation model is used. The ones that have no implicit solvation are shown in Figure 9.

−9.62 eV and −9.46 eV for two Al systems. In both cases this gap can be attributed to the lack of an Al atom in connecting 4MR for the high formation energy structures.

Interestingly distributions where Al pairs occupy the same 4MR are not favorable when we examine the fully formed SSZ-39 crystal which indicates SSZ-39 may have different Al distributions depending on whether the Al distribution is determined by kinetic or thermodynamic factors with kinetic factors favoring Al pairs in 4MRs while thermodynamic factors favor Al pairs in 6MRs and 8MRs.

It is important to note that this analysis relies on the assumption that the connection of D6MR subunits is a useful descriptor for the kinetics of SSZ-39 formation. This assumption could be reasonably challenged by pointing to sources claiming the D6MRs dissolve during the interconversion of FAU to other zeolite structures,[14] proposing alternative nucleation pathways or arguing the kinetics of SSZ-39 formation are influenced by other factors such as the dissolution rate of FAU. Since this assumption may be incorrect these results should primarily be interpreted as showing that thermodynamic favorability for a specific Al distribution does not necessarily translate into kinetic favorability for the Al distribution.

4. CONCLUSIONS

The energetics of 26 different Al distributions in SSZ-39 were tested when charge compensated by various combinations of *N*,*N*-dimethyl-3-5-dimethylpiperidinium isomers and sodium atoms. Ground state energies were found to correlate with N−Al distance when the OSDA was frozen in the ideal position for a chargeless OSDA. However, since *N*,*N*-dimethyl-3-5-dimethylpiperidinium is capable of reorienting in SSZ-39 nearly all optimized configurations contain N−Al distances in the 4.5−5.5 Å range meaning the differences in energies observed are likely due to interactions between the OSDA and the zeolite framework rather than anion−cation distances. The wide varieties of orientations available to *N*,*N*-dimethyl-3-5-dimethylpiperidinium meant local minima were quite common and required methods to screen multiple initial orientations. Using NWPEsSE to generate large numbers of initial OSDA orientations and screening them with single point calculations and geometry optimizations using force field calculations enabled the identification of more stable configurations compared to when OSDA placement was based on chemical intuition. The distortion energy was found to prohibit having

https://doi.org/10.1021/acs.chemmater.4c02175
Chem. Mater. 2024, 36, 11852−11862

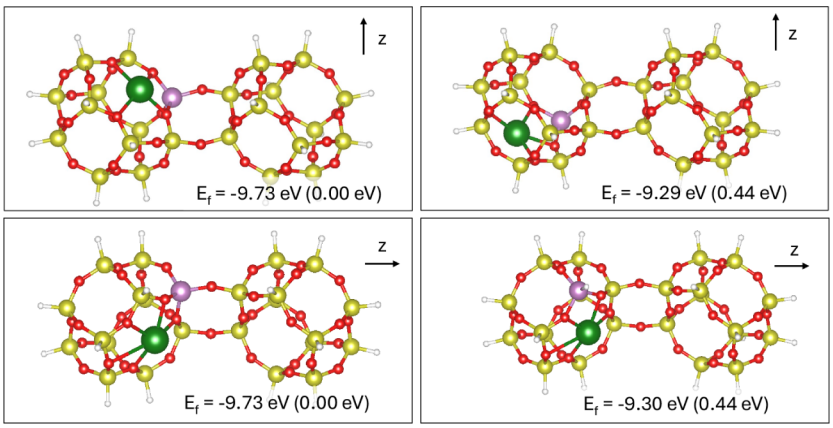

Figure 17. Best and second-best configurations for two D6MR subunits and one Al that is charge compensated by one Na cation. The two most favorable configurations have one Al atom linking the two subunits either perpendicular (top left panel) or parallel to the *z* axis (bottom left panel). The two second-best configurations do not have an Al linking the two D6MR (top and right bottom right panels). Formation energies are given in the bottom right and ground state energies are given in parentheses. Ground state energies are relative to the lowest energy for a given connection which has been set to zero.

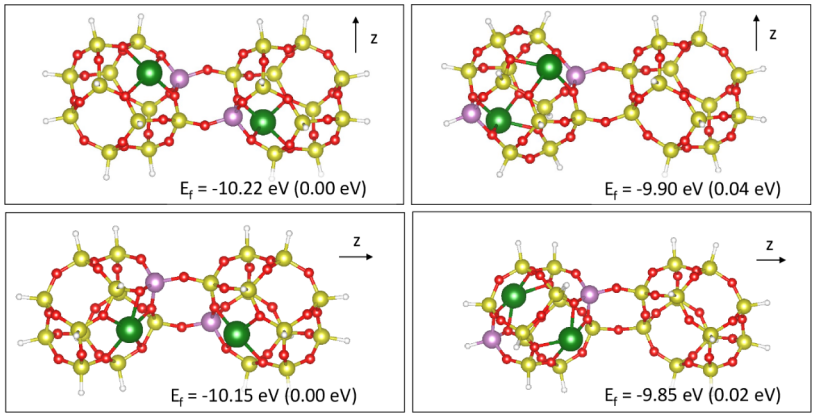

Figure 18. Best and second-best configurations for two D6MR subunits with two Al atoms that are charge compensated by two Na cations. The most favorable configurations have two Al atoms linking the D6MR (top and bottom left panels), The two second-best configurations have only one Al linking the two subunits (top and bottom right panels) with both Na cations bonded to the same D6MR unit. Formation energies are given in the bottom right and ground state energies are given in parentheses. Ground state energies are relative to the lowest energy for a given connection which has been set to zero.

two OSDAs occupy the same cage in SSZ-39. The isomer of *N*,*N*-dimethyl-3-5-dimethylpiperidinium can have a significant impact on the ground state energies of different Al distributions in SSZ-39. *Trans* OSDAs were found to favor the placement of Al pairs in 8 membered rings while *cis* OSDAs favored placing Al pairs in double six membered rings or in separate subunits. The presence of Na was found to favor Al pairs in six membered rings. Ground state energies for charge compensated SSZ-39 systems did not correlate with bare SSZ-39 systems indicating changes in energy were due to interactions between the zeolite and the charge compensating species rather than certain Al distributions being inherently more stable. Implicit solvation models were found to have minimal impacts on the energies and geometries of systems only containing OSDAs as charge compensating species. When systems containing Na were reoptimized using implicit solvation models, the most favorable position for Na shifted from a 6MR to an empty SSZ-39 cage resulting in significant changes in energy. The ideal Al pair distributions identified by evaluating the formation energy of SSZ-39 building blocks were found to be different than the ideal Al pair distributions identified by evaluating the energetics of Al pairs in SSZ-39 when charge compensated by various charge compensating species indicating kinetic control and thermodynamic control of Al distributions in SSZ-39 produce different Al distributions.

■ ASSOCIATED CONTENT

Supporting Information

The Supporting Information is available free of charge at https://pubs.acs.org/doi/10.1021/acs.chemmater.4c02175.

Structure of SSZ-39 and T site location in SSZ-39; comparison of energies calculated by LAMMPS to energies calculated by VASP; total energy as a function of volume; workflow for OSDA-zeolite structure generation and optimization; comparison of energies of SSZ-39 when charge compensated by a background charge to energies when charge compensated by OSDA species; aluminum pair distributions tested; ideal OSDA orientations in chargeless systems, connected D6MR formation energies (PDF)

Crystallographic data for a DFT-based structure (CIF)

https://doi.org/10.1021/acs.chemmater.4c02175
Chem. Mater. 2024, 36, 11852−11862

AUTHOR INFORMATION

Corresponding Author

Jean-Sabin McEwen − *The Gene and Linda Voiland School of Chemical Engineering and Bioengineering, Washington State University, Pullman, Washington 99164, United States; Institute for Integrated Catalysis, Pacific Northwest National Laboratory, Richland, Washington 99352, United States; Department of Physics and Astronomy, Department of Chemistry, and Department of Biological Systems Engineering, Washington State University, Pullman, Washington 99164, United States;* orcid.org/0000-0003-0931-4869; Email: js.mcewen@wsu.edu

Authors

Charles E. Umhey − *The Gene and Linda Voiland School of Chemical Engineering and Bioengineering, Washington State University, Pullman, Washington 99164, United States*

Jiawei Guo − *Department of Chemical Engineering, University of California, Davis, California 95616, United States;* orcid.org/0000-0001-9373-4297

Zheng Cui − *Department of Chemical and Biomolecular Engineering, Tulane University, New Orleans, Louisiana 70118, United States*

Daniel F. Shantz − *Department of Chemical and Biomolecular Engineering, Tulane University, New Orleans, Louisiana 70118, United States;* orcid.org/0000-0002-3237-6120

Ambarish Kulkarni − *Department of Chemical Engineering, University of California, Davis, California 95616, United States;* orcid.org/0000-0001-9834-8264

Complete contact information is available at: https://pubs.acs.org/10.1021/acs.chemmater.4c02175

Notes

The authors declare no competing financial interest.

ACKNOWLEDGMENTS

The authors acknowledge NSF grant CBET-2035302 and CBET-2035280 for support. C.U. also acknowledges partial funding from the CeRCaS NSF IUCRC under grant number CBET-1939876. This work was partially funded by the Joint Center for Deployment and Research in Earth Abundant Materials (JCDREAM) in Washington State. This work also used Bridges-2 at the Pittsburgh Supercomputer Center through allocation CHE170068 from the Advanced Cyberinfrastructure Coordination Ecosystem: Services & Support (ACCESS) program, which is supported by National Science Foundation grants #2138259, #2138286, #2138307, #2137603, and #2138296.[41] Additional computational resources were provided by the Kamiak HPC under the Center for Institutional Research Computing at Washington State University. The Pacific Northwest National Laboratory is operated by Battelle for the U.S. DOE.

REFERENCES

(1) Vermeiren, W.; Gilson, J. P. Impact of Zeolites on the Petroleum and Petrochemical Industry. *Top. Catal.* **2009**, *52*, 1131−1161.

(2) Wang, S.; Peng, Y. Natural Zeolites as Effective Adsorbents in Water and Wastewater Treatment. *Chem. Eng. J.* **2010**, *156*, 11−24.

(3) Qi, X.; Wang, Y.; Liu, C.; Liu, Q. The Challenges and Comprehensive Evolution of Cu-Based Zeolite Catalysts for SCR Systems in Diesel Vehicles: A Review. *Catal. Surv. Asia* **2023**, *27*, 181−206.

(4) Dědeček, J.; Sobalík, Z.; Wichterlová, B. Siting and Distribution of Framework Aluminium Atoms in Silicon-Rich Zeolites and Impact on Catalysis. *Catal. Rev.: Sci. Eng.* **2012**, *54*, 135−223.

(5) Lee, H.; Kim, J.; Song, I.; Jeon, S. W.; Cho, S. J.; Kim, D. H. Controlling the Distribution of Aluminum in a Cu−Zeolite Catalyst by Seed-Assisted Synthesis to Improve Its NH_3 -SCR Activity. *Catal. Sci. Technol.* **2022**, *12*, 7470−7480.

(6) Moliner, M.; Franch, C.; Palomares, E.; Grill, M.; Corma, A. Cu−SSZ-39, an Active and Hydrothermally Stable Catalyst for the Selective Catalytic Reduction of NO_x. *Chem. Commun.* **2012**, *48*, 8264−8266.

(7) Dusselier, M.; Davis, M. E. Small-Pore Zeolites: Synthesis and Catalysis. *Chem. Rev.* **2018**, *118*, 5265−5329.

(8) Ransom, R.; Moulton, R.; Shantz, D. F. The Structure Directing Agent Isomer Used in SSZ-39 Synthesis Impacts the Zeolite Activity towards Selective Catalytic Reduction of Nitric Oxides. *J. Catal.* **2020**, *382*, 339−346.

(9) Ransom, R.; Coote, J.; Moulton, R.; Gao, F.; Shantz, D. F. Synthesis and Growth Kinetics of Zeolite SSZ-39. *Ind. Eng. Chem. Res.* **2017**, *56*, 4350−4356.

(10) Dusselier, M.; Schmidt, J. E.; Moulton, R.; Haymore, B.; Hellums, M.; Davis, M. E. Influence of Organic Structure Directing Agent Isomer Distribution on the Synthesis of SSZ-39. *Chem. Mater.* **2015**, *27*, 2695−2702.

(11) Schwalbe-Koda, D.; Kwon, S.; Paris, C.; Bello-Jurado, E.; Jensen, Z.; Olivetti, E.; Willhammar, T.; Corma, A.; Román-Leshkov, Y.; Moliner, M. A Priori Control of Zeolite Phase Competition and Intergrowth with High-Throughput Simulations. *Science* **2021**, *374*, 308−315.

(12) Wang, X.; Wang, Y.; Moini, A.; Gounder, R.; Maginn, E. J.; Schneider, W. F. Influence of an N, N, N -Trimethyl-1-Adamantyl Ammonium ($TMAda^+$) Structure Directing Agent on Al Distributions and Pair Features in Chabazite Zeolite. *Chem. Mater.* **2022**, *34*, 10811−10822.

(13) Di Iorio, J. R.; Li, S.; Jones, C. B.; Nimlos, C. T.; Wang, Y.; Kunkes, E.; Vattipalli, V.; Prasad, S.; Moini, A.; Schneider, W. F.; Gounder, R. Cooperative and Competitive Occlusion of Organic and Inorganic Structure-Directing Agents within Chabazite Zeolites Influences Their Aluminum Arrangement. *J. Am. Chem. Soc.* **2020**, *142*, 4807−4819.

(14) Muraoka, K.; Sada, Y.; Shimojima, A.; Chaikittisilp, W.; Okubo, T. Tracking the Rearrangement of Atomic Configurations during the Conversion of FAU Zeolite to CHA Zeolite. *Chem. Sci.* **2019**, *10*, 8533−8540.

(15) Zhang, J.; Chu, Y.; Liu, X.; Xu, H.; Meng, X.; Feng, Z.; Xiao, F.-S. Interzeolite Transformation from FAU to CHA and MFI Zeolites Monitored by UV Raman Spectroscopy. *Chin. J. Catal.* **2019**, *40*, 1854−1859.

(16) Inagaki, S.; Tsuboi, Y.; Nishita, Y.; Syahylah, T.; Wakihara, T.; Kubota, Y. Rapid Synthesis of an Aluminum-Rich MSE-Type Zeolite by the Hydrothermal Conversion of an FAU-Type Zeolite. *Chem. - Eur. J.* **2013**, *19*, 7780−7786.

(17) Kwak, S. J.; Kim, H. S.; Park, N.; Park, M.-J.; Lee, W. B. Recent Progress on Al Distribution over Zeolite Frameworks: Linking Theories and Experiments. *Korean J. Chem. Eng.* **2021**, *38*, 1117−1128.

(18) Paolucci, C.; Parekh, A. A.; Khurana, I.; Di Iorio, J. R.; Li, H.; Albarracin Caballero, J. D.; Shih, A. J.; Anggara, T.; Delgass, W. N.; Miller, J. T. Catalysis in a Cage: Condition-Dependent Speciation and Dynamics of Exchanged Cu Cations in SSZ-13 Zeolites. *J. Am. Chem. Soc.* **2016**, *138*, 6028−6048.

(19) Shan, Y.; Shan, W.; Shi, X.; Du, J.; Yu, Y.; He, H. A Comparative Study of the Activity and Hydrothermal Stability of Al-Rich Cu-SSZ-39 and Cu-SSZ-13. *Appl. Catal., B* **2020**, *264*, 118511.

(20) Thompson, A. P.; Aktulga, H. M.; Berger, R.; Bolintineanu, D. S.; Brown, W. M.; Crozier, P. S.; In't Veld, P. J.; Kohlmeyer, A.; Moore, S. G.; Nguyen, T. D. LAMMPS - a Flexible Simulation Tool for Particle-Based Materials Modeling at the Atomic, Meso, and Continuum Scales. *Comput. Phys. Commun.* **2022**, *271*, 108171.

(21) Mayo, S. L.; Olafson, B. D.; Goddard, W. A. DREIDING: A Generic Force Field for Molecular Simulations. *J. Phys. Chem.* **1990**, *94*, 8897−8909.
(22) Wang, X.; Wang, Y.; Moini, A.; Gounder, R.; Maginn, E. J.; Schneider, W. F. Influence of an N,N,N-Trimethyl-1-adamantyl Ammonium (TMAda+) Structure Directing Agent on Al Distributions and Pair Features in Chabazite Zeolite. *Chem. Mater.* **2022**, *34*, 10811−10822.
(23) Boulfelfel, S. E.; Findley, J. M.; Fang, H.; Daou, A. S. S.; Ravikovitch, P. I.; Sholl, D. S. A Transferable Force Field for Predicting Adsorption and Diffusion of Small Molecules in Alkali Metal Exchanged Zeolites with Coupled Cluster Accuracy. *J. Phys. Chem. C* **2021**, *125*, 26832−26846.
(24) Kresse, G.; Furthmüller, J. Efficient Iterative Schemes for Ab Initio Total-Energy Calculations Using a Plane-Wave Basis Set. *Phys. Rev. B* **1996**, *54*, 11169−11186.
(25) Kresse, G.; Furthmüller, J. Efficiency of Ab-Initio Total Energy Calculations for Metals and Semiconductors Using a Plane-Wave Basis Set. *Comput. Mater. Sci.* **1996**, *6*, 15−50.
(26) Kresse, G.; Hafner, J. Ab Initio Molecular Dynamics for Liquid Metals. *Phys. Rev. B* **1993**, *47*, 558−561.
(27) Kresse, G.; Joubert, D. From Ultrasoft Pseudopotentials to the Projector Augmented-Wave Method. *Phys. Rev. B* **1999**, *59*, 1758−1775.
(28) Lejaeghere, K.; Bihlmayer, G.; Björkman, T.; Blaha, P.; Blügel, S.; Blum, V.; Caliste, D.; Castelli, I. E.; Clark, S. J.; Dal Corso, A. Reproducibility in Density Functional Theory Calculations of Solids. *Science* **2016**, *351*, 1415−1423.
(29) Klimeš, J.; Bowler, D. R.; Michaelides, A. Van Der Waals Density Functionals Applied to Solids. *Phys. Rev. B* **2011**, *83*, 195131.
(30) Wang, V.; Xu, N.; Liu, J. C.; Tang, G.; Geng, W. T. VASPKIT: A User-Friendly Interface Facilitating High-Throughput Computing and Analysis Using VASP Code. *Comput. Phys. Commun.* **2021**, *267*, 108033.
(31) Mathew, K.; Kolluru, V. C.; Hennig, R. G.*VASPsol: Implicit Solvation and Electrolyte Model for Density-Functional Theory*GitHub2018
(32) Mathew, K.; Kolluru, V. S. C.; Mula, S.; Steinmann, S. N.; Hennig, R. G. Implicit Self-Consistent Electrolyte Model in Plane-Wave Density-Functional Theory. *J. Chem. Phys.* **2019**, *151*, 234101.
(33) Mathew, K.; Sundararaman, R.; Letchworth-Weaver, K.; Arias, T. A.; Hennig, R. G. Implicit Solvation Model for Density-Functional Study of Nanocrystal Surfaces and Reaction Pathways. *J. Chem. Phys.* **2014**, *140*, 084106.
(34) Baelocher, C.; McCusker, L. B. *Database of Zeolite Structures*. IZA.
(35) Antonio, D. D.; Guo, J.; Holton, S. J.; Kulkarni, A. R. Simplifying Computational Workflows with the Multiscale Atomic Zeolite Simulation Environment (MAZE). *SoftwareX* **2021**, *16*, 100797.
(36) Zhang, J.; Dolg, M. ABCluster: The Artificial Bee Colony Algorithm for Cluster Global Optimization. *Phys. Chem. Chem. Phys.* **2015**, *17*, 24173−24181.
(37) Zhang, J.; Dolg, M. Global Optimization of Clusters of Rigid Molecules Using the Artificial Bee Colony Algorithm. *Phys. Chem. Chem. Phys.* **2016**, *18*, 3003−3010.
(38) Zhang, J.; Glezakou, V.-A.; Rousseau, R.; Nguyen, M.-T. NWPEsSe: An Adaptive-Learning Global Optimization Algorithm for Nanosized Cluster Systems. *J. Chem. Theory Comput.* **2020**, *16*, 3947−3958.
(39) Randrianandraina, J.; Badawi, M.; Cardey, B.; Grivet, M.; Groetz, J.-E.; Ramseyer, C.; Anzola, F.; Chambelland, C.; Ducret, D. Adsorption of water in Na-LTA zeolites: An ab initio molecular dynamics investigation. *Phys. Chem. Chem. Phys.* **2021**, *23*, 19032−19042.
(40) Faux, D. A.; Smith, W.; Forester, T. R. Molecular Dynamics Studies of Hydrated and Dehydrated Na^+-Zeolite-4A. *J. Phys. Chem. B* **1997**, *101*, 1762−1768.
(41) Boerner, T. J.; Deems, S.; Furlani, T. R.; Knuth, S. L.; Towns, J. ACCESS: Advancing Innovation. In *Practice and Experience in Advanced Research Computing*; ACM: New York, NY, USA, 2023; pp 173−176.

https://doi.org/10.1021/acs.chemmater.4c02175
Chem. Mater. 2024, 36, 11852−11862